Dynamic Colocalization Microscopy To Characterize Intracellular Trafficking of Nanomedicines

Dries Vercauteren,[†,‡] Hendrik Deschout,[†,‡] Katrien Remaut,[†] Johan F.J. Engbersen,[§] Arwyn T. Jones,[⊥] Jo Demeester,[†] Stefaan C. De Smedt,[†,*] and Kevin Braeckmans[†,‡]

[†]Laboratory of General Biochemistry and Physical Pharmacy, and [‡]Centre for Nano- and Biophotonics, Ghent University, Harelbekestraat 72, B-9000 Ghent, Belgium, [§]Department of Biomedical Chemistry, MIRA Institute for Biomedical Technology and Technical Medicine, Faculty of Science and Technology, University of Twente, P.O. Box 217, 7500 AE Enschede, The Netherlands, and [⊥]Welsh School of Pharmacy, Redwood Building, Cardiff University, CF10 3NB, Cardiff, Wales

ABSTRACT To gain a better understanding of intracellular processing of nanomedicines, we employed quantitative live-cell fluorescence colocalization microscopy to study endosomal trafficking of polyplexes in retinal pigment epithelium cells. A new, dynamic colocalization algorithm was developed, based on particle tracking and trajectory correlation, allowing for spatiotemporal characterization of internalized polyplexes in comparison with endosomal compartments labeled with EGFP constructs. This revealed early trafficking of the polyplexes specifically to Rab5- and flotillin-2-positive vesicles and subsequent delivery to Rab7 and LAMP1-labeled late endolysosomes where the major fraction of the polyplexes remains entrapped for days, suggesting the functional loss of these nanomedicines. Colocalization of polyplexes with the autophagy marker LC3 suggests for the first time that the process of xenophagy could play an important role in the persistent endosomal entrapment of nanomedicines.

KEYWORDS: nanomedicines · nonviral ocular gene therapy · particle tracking · intracellular trafficking · colocalization · autophagy

Advanced pharmaceutical nanoparticles for controlled delivery of drug molecules or biopharmaceuticals are an important class of nanomedicines. The multifunctional carrier in these nanomedicines helps controlling drug biodistribution, stability of the therapeutic payload, and enhancing its specific release at the desired location of action. For an increasing number of therapeutics the target is intracellular and the therapeutic itself is often membrane impermeable as it is the case for nucleic acids.[1] Hence, the carrier molecules are also responsible for traversing the intrinsic cellular barriers and releasing the therapeutics at the appropriate subcellular location. One approach is to take advantage of the endosomal system, which forms a natural entry route into the cell.[2] Immediately following endocytic uptake, further intracellular sorting of the endocytic vesicles and trafficking will dictate the intracellular fate of the associate therapeutics, involving cargo selection, vesicle budding, active transport of the endosomes, vesicle docking and fusion events, all tightly regulated by, for example, proteins of the Rab GTPase family.[3] A subset of the endosomes will mature to form late endosomes, characterized by a significant reduction in luminal pH and the formation of multivesicular bodies that can fuse with lysosomes in order to degrade the content.[4] These so-called endolysosome hybrid organelles are considered to be the terminal degradative compartment of the endocytic pathway. The endosomal sorting process is strongly dependent on the nature of both the target cell[5] and functionalization of the carrier.[1,6]

More specifically, gene therapy requires nucleic acid delivery to the cytosol or even cell nucleus when transcription of the therapeutic nucleic acids is required. Therefore, after endocytosis, nanomedicines for nucleic acid delivery need to assist in the endosomal release of the large hydrophilic nucleic acids into the cytosol. This before the bulk of the nucleic acids is delivered to the endolysosomes and the protective carrier dissociates from the nucleic acid, exposing the latter to enzymatic degradation by the acid hydrolases. Several different strategies have been described as attempts to enhance endosomal release.[1] Despite this, the entrapment and degradation of nucleic acid nanomedicines in endolysosomal compartments are currently considered as major barriers for cytosolic nucleic acid delivery and are, to a large extent, responsible for the low transfection efficiency of nonviral nucleic acid carriers compared with their viral counterparts.[7,8] To further improve subcellular delivery of nucleic acids, it is essential to obtain a better understanding of the intracellular sorting of nucleic acid delivery vehicles. Fluorescence colocalization microscopy has been used to some

* Address correspondence to Stefaan.DeSmedt@UGent.be.

Received for review June 7, 2011 and accepted September 17, 2011.

Published online September 18, 2011
10.1021/nn2020858

degree to study these processes *via* fluorescent labeling of both the nanomedicines and specific cell organelles. This is often done in fixed cells using direct fluorescence or immunostaining techniques.[9] However, this approach can cause fixation artifacts,[10] in particular related to the spatial distribution of the gene carriers.[11] Moreover, this approach does not easily provide information on the kinetics of colocalization, as opposed to live-cell imaging. Due to the advent of fluorescent proteins and technical developments in fluorescence microscopy, time lapse imaging of live cells is becoming the preferred method.[12,13]

In this work, we have used quantitative live-cell fluorescence colocalization microscopy to study the intracellular trafficking of polymeric gene complexes (polyplexes) in living retinal pigment epithelium (RPE) cells, being attractive targets for ocular gene therapy.[14] The polymeric vector in this study is the linear, bioreducible, poly(amido amine) poly(*N*,*N*′-cystaminebisacrylamide 4-aminobutanol) (p(CBA-ABOL)),[15,16] a class of polymers which has shown great promise for nucleic acid transfer and protein delivery in different cell types.[17−21] In a recent study we have found that these polyplexes are taken up in RPE cells by endocytic processes requiring flotillin-1 and PAK-1.[22] The present work is aimed at elucidating the subsequent intracellular processing of p(CBA-ABOL)/DNA polyplexes inside living ARPE-19 cells after labeling diverse endocytic organelles by EGFP constructs of clathrin, Rab5, Rab11, Rab7, LAMP-1, caveolin-1 (Cav1), flotillin-2 (Flot2) and LC3.

RESULTS

Validation of the Dynamic Colocalization Algorithm. No established quantitative method is currently available that takes advantage of the time information of single objects in fluorescence movies for the quantification of colocalization. The advantage of using not only spatial but also temporal information was pointed out previously in a study on the interaction of membrane proteins.[23] Here we build forth on this concept and present a new quantitative method for the detection of correlated movement, which is a convincing proof of the interaction of two objects. Therefore, a novel colocalization algorithm was developed, based on particle tracking (SPT)[24−27] and correlated movement of object trajectories (see also Theory section in Supporting Information and supplemental Figure 1), here referred to as dynamic colocalization.

To validate whether the dynamic colocalization algorithm can detect colocalization based on correlated movement, the method was compared to classic pixel- and object-based colocalization on dual-color live-cell microscopy movies of endocytosed polystyrene multicolor Tetraspeck microspheres (see Methods). Figure 1A shows a single frame of an overlay movie, clearly showing

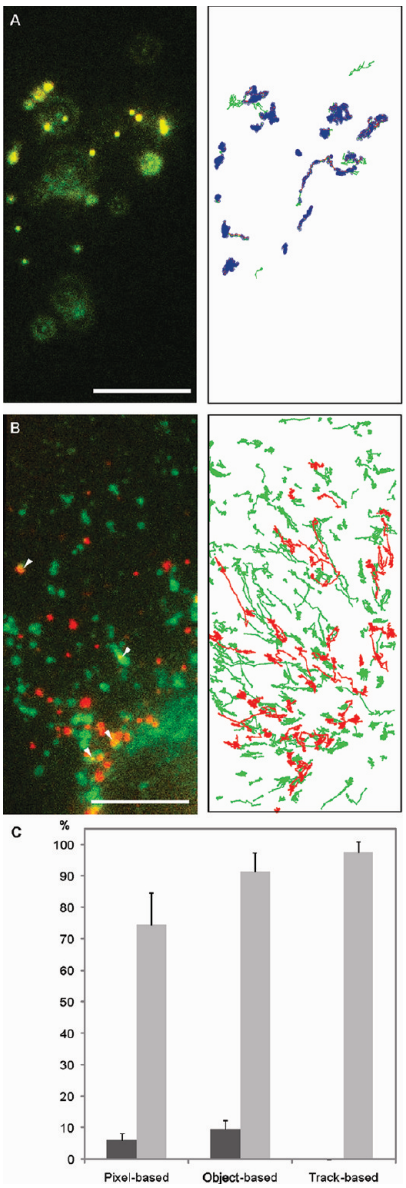

Figure 1. Validation of the dynamic colocalization algorithm and comparison with pixel- and object-based colocalization coefficient. As a positive control for colocalization, movies of endocytosed multicolor Tetraspec microspheres were acquired. As a negative control, the red channel of a set of movies, corresponding to p(CBA-ABOL) polyplexes, were shuffled before overlay with the green channels from the same experiment, corresponding to EGFP-LAMP1 expression. This resulted in an overlay of endosome and polyplex signals that were taken in different cells, showing no correlated movement. (A) Exemplary overlay image of intracellular Tetraspec beads and the corresponding trajectories from that movie. Scale bar is 10 μm. (B) Exemplary image of a cell expressing EGFP-LAMP1 overlaid with in image of red polyplexes from a different cell. Accidental colocalization in regions with a high particle density of green and red objects is highlighted with a white arrowhead. Corresponding trajectories of the green and red objects are shown in the right. Scale bar is 10 μm. (C) The percentage of colocalization, calculated with the three different algorithms, based on pixels, objects and trajectories on both the positive control (gray bars) and the negative control (black bars). Averages of a single experiment are shown (N = 10) and error bars represent standard deviations.

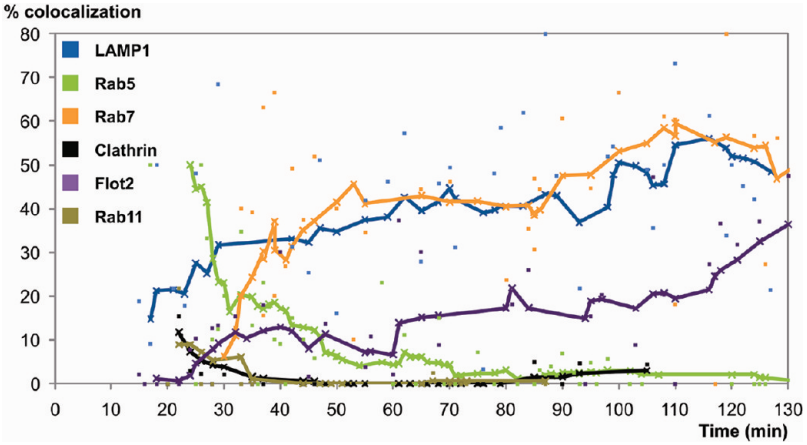

Figure 2. The intracellular endocytic trafficking profile of 10 kDa dextran in ARPE-19 cells. Trajectory-based dynamic colocalization of fluorescent dextran with the endosomal markers Rab5 (green), light-chain clathrin (black), Rab11 (khaki), Flot2 (purple), Rab7 (orange), and LAMP1 (blue) was calculated and plotted in function of time (dots). Every dot corresponds to a movie that was taken in a different cell at that time point. To improve the visibility of the trend, track-weighted running averages with a window of 5 consecutive time points were calculated and plotted as a solid line.

100% colocalization, next to a plot of the corresponding trajectories. The pairs of green and red tracks that are found to be correlated according to the dynamic colocalization algorithm are highlighted in blue. As a negative control, dual-color fluorescence movies without correlated movement of fluorescent objects were obtained by a random overlay of the red channels (polyplexes) with the green channels (endosomes) from different cells. An example of which is shown in Figure 1B. While, in individual frames of the movie, some polyplexes might colocalize with endosomes by chance in regions with a high particle density where green and red objects are very close to one another (Figure 1B, white arrowheads), none of the polyplexes should show correlated movement with the endosomes. For both the positive and negative control, fluorescence colocalization was then calculated with the three colocalization algorithms. For the pixel- and object-based algorithms, the depicted colocalization coefficient for a single movie was obtained by averaging the colocalization coefficients over the 120 frames of the movie, therefore already including a time-component, in contrast to static colocalization (see also Supporting Information, Figure 2). In the case of dynamic track-based colocalization, we constructed the trajectories of all green and red objects in a single movie by means of SPT and quantified the ratio of red tracks that correlate with green tracks. Figure 1C shows the results from analyzing 10 movies. The track-based colocalization algorithm gives the best estimate of the true colocalization (97.6 $\pm$ 3.3%), followed by the object- (91.4 $\pm$ 5.9%) and pixel-based (74.4 $\pm$ 10.2%) methods (Figure 1C, gray bars). Pixel-based colocalization clearly underestimates the actual colocalization because of its higher sensitivity to background noise (see Supporting Information and supplemental Figure 2). For the negative control, as expected, both pixel-based and object-based colocalization algorithms showed a significant number of false positives, due to the incidental overlap of green and red objects (Figure 1C, black bars). The new dynamic colocalization method on the other hand showed no false positive colocalization since it specifically searches for correlated movement. Taken together, the trajectory-based colocalization algorithm is the most accurate in identifying true colocalization and is the least prone to the detection of false positives. Therefore, we conclude that dynamic colocalization is an attractive tool to quantify colocalization in dual-color fluorescence time-lapse acquisitions of living cells.

Postendocytic Trafficking of 10 kDa Dextran in Living ARPE-19 cells. As a first demonstration that trajectory-based colocalization allows for careful scrutiny of the intracellular trafficking of endocytic ligands, we followed intracellular processing of fluorescently labeled 10 kDa dextran, representing a well-characterized endocytic probe. Large hydrophilic dextran molecules are internalized *via* fluid-phase endocytosis and trafficked to endolysosomes.[27,28] We studied colocalization in ARPE-19 cells of dextran with clathrin-coated vesicles (EYFP-Clathrin), recycling endosomes (EGFP-Rab11), early endosomes (GFP-Rab5), Flot2 (EGFP-Flot2), late endosomes (EGFP-Rab7), and lysosomes or endolysosomal hybrid organelles (EGFP-LAMP1). At 24 h after transfection with the fluorescent fusion proteins, the cells were incubated for 15 min with red fluorescent dextran, after which the cells were washed with cell culture medium and imaged for 2 h on the SPT-microscope. For every time point, a new cell with a low GFP expression level was selected to minimize phototoxicity and to obtain information on a large population of cells. Particle tracking and dynamic colocalization with Clathrin, Rab5, Rab11, Rab7, Flot2, and LAMP1 was then calculated off-line, the results of which are shown in Figure 2 (dots). To visualize the main trend (Figure 2, lines), a running average, weighted for the amount of

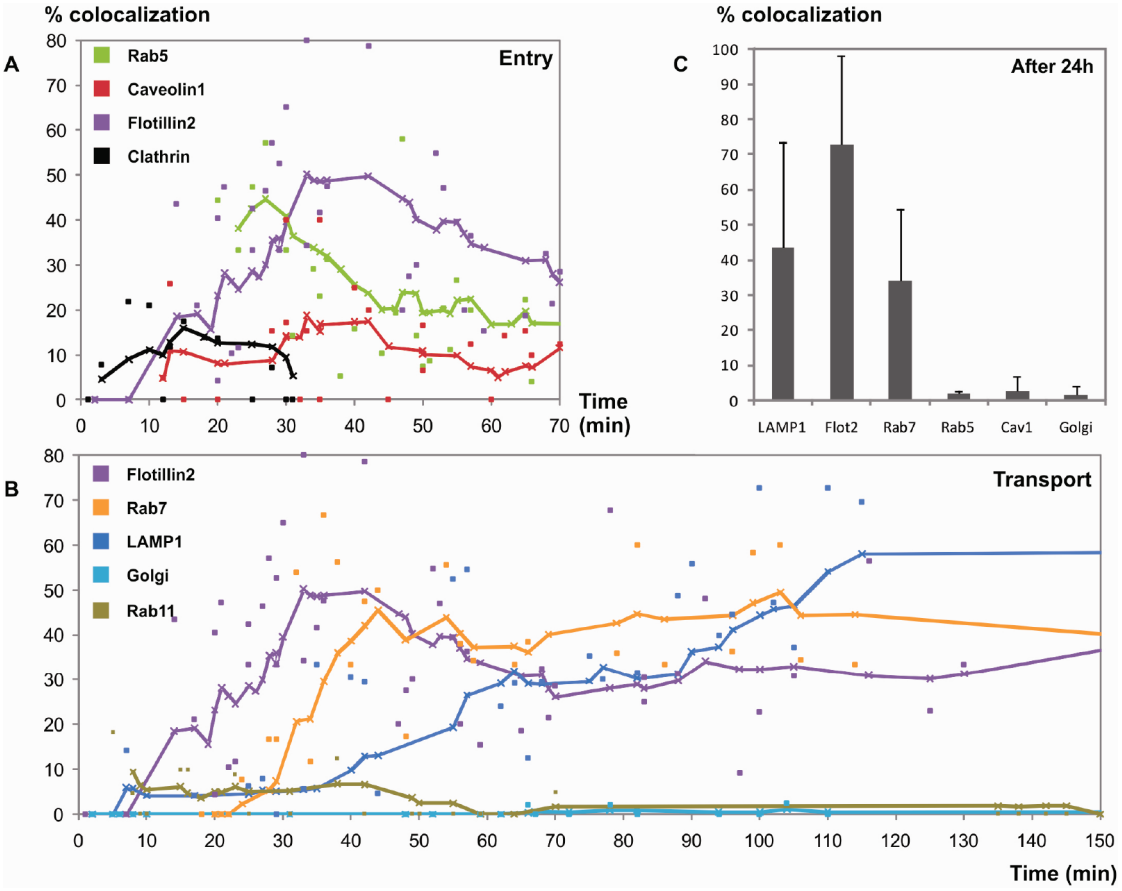

Figure 3. The intracellular endocytic trafficking profile of p(CBA-ABOL) polyplexes in ARPE-19 cells.The percentage of polyplexes that colocalize with (A) early endosomal markers (Cav1, Rab5, Clathrin, and Flotillin2) and (B) late endosomal markers (LAMP1, Rab7, Golgi, Flotillin2, Rab11), obtained with the dynamic, trajectory-based colocalization algorithm is shown. Dynamic colocalization values were calculated at every indicated time point (dots) and the corresponding running averages, weighted to the amount of red tracks, are plotted to show the main colocalization trends (lines). All experiments were repeated twice and all colocalization results were pooled to build the trend line. (C) Average dynamic colocalization of the polyplexes with the different endosomal markers, 24 h after their administration ($N = 5$). Error bars are standard deviations.

polyplex trajectories that were detected in the individual movies, was applied (see also Methods). As expected, at early time points, most of the dextran is found in Rab5-positive (Rab5+) early endosomes (Figure 2, green) and is subsequently trafficked to Rab7+ and LAMP1+ organelles (Figure 2, orange and blue). We note that a fraction of these Rab5+, dextran-containing vesicles exhibit diameters of several micrometers, suggesting they represent macropinosomes formed following constitutive macropinocytosis (Supporting Information, Figure 5). Only very little colocalization of dextran with recycling endosomes (Rab11-GFP, khaki) and clathrin-coated vesicles (Clathrin-YFP, black) was observed at early measured time points. The colocalization with Flot2 increased steadily to approximately 35% after 2 h (Figure 2, purple). These results demonstrate that the method of track-based dynamic colocalization opens new perspectives in the study of intracellular processing of endosomal ligands, allowing for quantitative assessment of colocalization kinetics.

Postendocytic Trafficking of Cationic p(CBA-ABOL)/DNA Polyplexes in Living ARPE-19 Cells. Having established that track-based dynamic colocalization is a useful approach to study intracellular trafficking kinetics of endocytic ligands, we proceeded to map the postendocytic trafficking profile of p(CBA-ABOL)/DNA polyplexes inside ARPE-19 cells. The study of these cationic polyplexes presented some extra challenges in quantifying colocalization, especially at the level of early postendocytic trafficking. Therefore, the trajectory-based colocalization algorithm was refined to meet these challenges (see Supporting Information Results and Figure 3). By defining a requirement of a minimum amount of movement, it became possible to exclude extracellular, plasma membrane attached objects from further analysis, which would be impossible to do for the classic pixel- and object-based colocalization analysis on single images. The trajectory-based protocol for colocalization analysis was subsequently applied to investigate the intracellular trafficking of cationic p(CBA-ABOL)/DNA polyplexes in ARPE-19 cells within different types of labeled endosomes. Separate

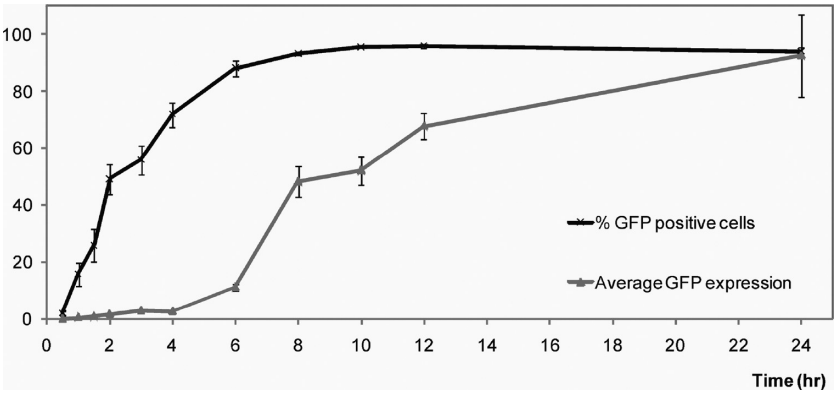

Figure 4. Kinetics of GFP reporter gene expression in ARPE-19 cells up to 24 h after transfection with p(CBA-ABOL)/mRNA polyplexes. Cells were incubated with a 48/1 ratio of p(CBA-ABOL)/GFP mRNA polyplexes in serum free conditions for 2 h. The cells were then washed and incubated in cell culture medium at 37 °C for various periods of time up to 24 h. At every time point, average GFP expression (gray line) and the percentage of GFP-positive cells (black line) were measured by flow cytometry. A single experiment was performed in triplicate and error bars represent standard deviations.

populations of cells were first transfected with one of eight various EGFP fusion proteins to label a specific subtype of endosomes. At 24 h later, p(CBA-ABOL)/Cy5-DNA polyplexes were added to the cells in OptiMEM and plasma membrane adhesion of the polyplexes was assured through repetitive pipetting at room temperature. The cells were then immediately washed with fresh OptiMEM and imaged on the SPT-microscope. Dual-color fluorescence movies were continuously acquired for at least two hours and also 24 h later. A new cell was selected for each movie to minimize phototoxicity and to obtain information on a large population of cells. An exemplary dual-color movie for every endosomal marker is given in Supporting Information (Videos 1−8). Particle tracking and dynamic colocalization was then calculated off-line and trendlines were plotted (Figure 3). The endosomal markers that are associated with cellular entry are shown in Figure 3A, the markers that are related to further intracellular trafficking or transport are shown in a separate plot (Figure 3B), and Figure 3C shows the average dynamic colocalization values that were measured, 24 h after administration of the polyplexes.

Dynamic colocalization analysis revealed a low association of clathrin-coated pits and polyplexes (Figure 3A, black), indicating that CDE does not play an essential role in polyplex endocytosis in ARPE-19 cells. Association with clathrin light-chain was assessed during the first 30 min because of its potential early role in endocytic processes. This finding is in accordance with our recent analysis of endocytosis of these gene complexes using pharmacological endocytic inhibitors and siRNA-mediated knockdown of specific endocytoc proteins and pathways.[22] Similar findings were obtained for Cav1-colocalization (Figure 3A, red), again in line with what we have previously found. A high colocalization of the polyplexes was observed with both Flot2 (purple) and Rab5 (green). This is expected as flotillin-mediated endocytosis (FlotME) was identified as being one of the major endocytic pathways through which these gene complexes are internalized.[22] The strong colocalization with Rab5 reveals trafficking of a fraction of the polyplexes to sorting endosomes, although Rab5 can also be associated with early macropinosomes or phagosomes.[3]

The association with Rab5 decreased over time in favor of Rab7 (orange) and LAMP1 (blue). This suggests that the polyplex-containing Rab5+ endosomes mature to late endosomes, since it is known that this is accompanied by an exchange of Rab5 for Rab7.[3] The increase in colocalization with LAMP1+ endosomes lags behind the increase with Rab7+ endosomes, which is strongly indicative of the fusion between late endosomes and lysosomes to initially form hybrid endolysosomes. After 2 h, the polyplexes localized primarily with LAMP1 and Rab7-labeled organelles, but interestingly, a significant fraction (±30%) of the polyplexes was still colocalizing with Flot2. High colocalization of the polyplexes with LAMP1 and Rab7 (40% on average) was still observed 24 h following their addition to cells (see Figure 3B). Surprisingly, a substantial colocalization with Flot2 of approximately 70% was still observed after 24 h. We note that percentages of colocalization of polyplexes with different endocytic markers at certain time points was found to exceed 100%. We suspect that this is due to a possible (partial) overlap between the different endosomal markers. It is for example known that Rab7+ vesicles intensively interact with LAMP1.[29] In addition, Figure 3B clearly shows that no colocalization up to 2 h was observed with the Golgi-apparatus (light blue), nor with Rab11+ recycling endosomes (khaki). Also after 24 h no colocalization with the Golgi-apparatus could be found.

Kinetics of mRNA Expression as a Measure for Endosomal Escape. Despite the high buffering capacity of p(CBA-ABOL), which is deemed to be responsible for efficient endosomal rupture and cytoplasmic release of the polyplexes,[15] our intracellular trafficking studies indicated that a large fraction of the polyplexes remains

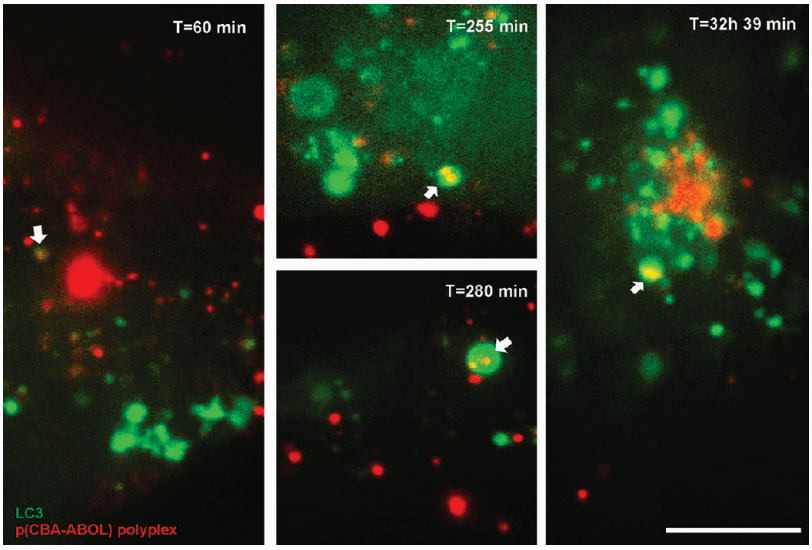

Figure 5. Role of xenophagy in the sequestration of polyplexes inside ARPE-19 cells. ARPE-19 cells were transfected with EGFP-LC3 (green), 24 h before exposure to p(CBA-ABOL)/Cy5-DNA polyplexes (red). Dual-color live-cell imaging was performed for 24 h after initial exposure to the polyplexes. Polyplexes were found in LC3+ endosomes at all time points. Scale bar is 10 μm.

trapped after 24 h inside LAMP1+ and Flot2+ vesicles and, therefore, probably do not contribute to the transfection of the cells. To investigate the time frame of cytoplasmic release of nucleic acids by the p(CBA-ABOL)-vector, we set up an experiment where we complexed p(CBA-ABOL) with mRNA coding for EGFP. Because this approach shortcuts nuclear translocation and transcription, and because of the bioreducible properties of the polymeric vector,[16] the expression profile should give an indication of the kinetics of cytoplasmic release of mRNA. p(CBA-ABOL)/mRNA polyplexes were prepared and added to ARPE-19 cells similar to the plasmid (pDNA) transfection protocol and washed away after 2 h. GFP expression was then measured at several time points. The results in Figure 4 show the highest increase in average GFP expression between 6 and 8 h postaddition to the cells, indicating that the intraendosomal mRNA is most likely to be escaping from the endosomes within this time period. The first evidence of GFP expression was already detectable between 30 and 60 min post-transfection, in agreement with other reports on mRNA transfection.[30] Moreover, we noticed that it took about 30 min to detect GFP in cells that were microinjected in the cytosol with these p(CBA-ABOL)/mRNA polyplexes (see Supporting Information Results and Figure 4). These results suggest that endocytic uptake of the polyplexes and endosomal escape can happen fairly quickly after addition of the polyplexes to the cells. Taken together, these data corroborate the presumption that the many polyplexes that remain trapped in vesicles after 24 h do not contribute to transfection.

The Involvement of an Autophagy-like Mechanism. The mechanism that is responsible for the persevering endosomal entrapment of the polyplexes remains, however, elusive. Some reports attribute endosomal entrapment of pathogenic invaders such as viruses and bacteria, to the involvement of an autophagy-like mechanism.[31] In this context, this mechanism is referred to as xenophagy and is believed to sequester both cytoplasmic xenogeneous particles as well as entire endosomes containing these pathogens.[32] Similar to the biogenesis of autophagosomes, the invader becomes enclosed by a phagophore, giving birth to a newly formed xenophagosome. Next, the xenophagosome matures, acquiring Rab7, and finally fuses with LAMP1 containing lysosomes, leading to the enzymatic degradation of the invader.[33] A cellular marker protein for the early and late xenophagosomes is the microtubule-associated protein 1A/1B-light chain 3 (LC3).[34] Colocalization kinetics of p(CBA-ABOL) polyplexes with EGFP-LC3 inside living ARPE-19 cells were investigated during 24 h after polyplex addition (see Supporting Information Figure 6). Figure 5 shows some colocalization of polyplex signals with LC3 in the first hour and at later time points, providing further evidence of the presence of polyplexes or possibly polyplex-containing endosomes inside large xenophagosomes. The movie is found in Supporting Information (Video 9). This is to the best of our knowledge, the first experimental proof that an autophagy-like mechanism is likely to be involved in the endosomal sequestration and possible degradation of gene complexes.

DISCUSSION

In the characterization of nanomedicines carrying payloads with intracellular targets, such as nucleic acid-carrying polyplexes or lipoplexes, little is known about their endosomal sorting once they are endocytosed. Yet, endosomal sorting will play a major role in determining

the efficiency of intracellular drug release and their final destiny. In this work we addressed this shortcoming by focusing on the *in vitro* intracellular processing of p(CBA-ABOL) polyplexes inside RPE cells, which have shown to be effective transfection agents *in vitro*.[15,17−22] Because of the dynamic nature of the intracellular endosomal sorting and the demonstrated incompatibility of standard fixation protocols with gene complexes, we selected live-cell imaging as the preferred experimental approach. However, mapping the kinetics of intracellular nanoparticle trafficking and subcellular localization remains a major challenge.

In this work, we introduced a quantitative approach to study live-cell endosomal colocalization dynamics of nanomedicines for gene delivery, which has several advantages over classic colocalization analysis methods designed for analyzing static images. This so-called dynamic colocalization algorithm looks for correlated motion of both nanomedicines and endosomes. The algorithm constructs trajectories of fluorescent objects which can represent both nanoparticles, agglomerates of nanoparticles, or microparticles, as particle tracking is independent of their size. In this way, trajectory correlation analysis avoids false assignment of colocalization between objects that are close to one another by mere coincidence. Moreover, the trajectories allow us to discriminate extracellular from internalized particles, based on a clear difference in mobility. We have shown that the trajectory-based colocalization analysis outperforms pixel- and object-based colocalization algorithms, both in terms of detecting true colocalization as well as avoiding false positives. As a validation of this method, we could successfully follow the well-characterized postendocytic trafficking of fluorescent dextran molecules by quantifying their dynamic colocalization with clathrin-coated pits, recycling endosomes, Flot2, Rab7, Rab5, and lysosomes. In a next step, trajectory-based dynamic colocalization was used to study the kinetics of the postendocytic processing of p(CBA-ABOL)/DNA polyplexes inside ARPE-19 cells, where these polyplexes have shown high *in vitro* transfection efficiencies.[22] While a low colocalization with clathrin and Cav1 was found, the polyplexes were clearly associated with Rab5+ endosomes at early time points that may represent early sorting endosomes, macropinosomes, and phagosomes.[3] Because of our previous finding that a significant part of these polyplexes is internalized *via* a phagocytosis-like mechanism,[22] there is the possibility that this colocalization is at least in part a result of the presence in Rab5+ early phagosomes. Furthermore, it is known that phagosomes mature by interchanging Rab5 for Rab7 and acquiring LAMP1 in a subsequent step due to lysosome fusion, giving rise to phagolysosomes.[4,35] This is in line with the observed increase in polyplex colocalization with Rab7 and then LAMP1, accompanied by a decrease in Rab5 colocalization. The involvement of phagocytosis is not surprising as it is known that the RPE exploit a highly developed phagolysosomal system, which is necessary for the engulfment and degradation of photoreceptor outer segments in the process of outer segment renewal.[36] Efficient phagocytosis-mediated digestion of polyplexes by RPE cells may therefore explain the low transfection efficiency of the polyplexes that are internalized *via* this endocytic pathway, as mentioned earlier.[22] Apart from Rab5, early colocalization with Flot2 was found, which confirms our recent findings that also FlotME plays an important role in the internalization of these polyplexes.[22] High colocalization with Rab7 and LAMP1 at late time points raises the question if polyplexes that have entered the cell *via* FlotME are also possibly directed to Rab7+ and LAMP1+ endolysosomes. Support for this hypothesis is found in the work by Payne *et al*. who reported that polyethylenimine (PEI)-polyplexes, internalized *via* a proteoglycan-mediated, flotillin-dependent endocytic pathway, are trafficked to Rab9+ late endosomes after 2 h,[37] wherefore it is conceivable that the flotillin mediated endocytic pathway merges with Rab7 and then LAMP1-labeled structures. Further support is found in recent work where flotillins were detected on acidic multivesicular bodies.[38] Lysosomal accumulation of exogenous nanomaterials seems to be quite universal since it was also reported for different types of nanoparticles like cationic polystyrene nanospheres or quantum dots.[6,39,40] Further research is necessary to determine why these nanoparticles remain trapped inside endolysosomes as this may help design new strategies for improving endosomal escape. In this work, the persistent and abundant presence of polyplexes inside LAMP1+ and Flot2+ endosomes after 24 h and the indication that the majority of endosomal escape occurs within the first 8 h after addition of the polyplexes to the cells, raised the question as to whether other mechanisms were responsible for the persisting endosomal sequestration of the polyplexes. To assess the involvement of autophagy/xenophagy during polyplex processing in RPE cells, recruitment of the autophagosomal marker protein LC3 to the polyplex-containing endosomes was evaluated. At different time points, polyplexes were observed to clearly colocalize with LC3, suggesting that the process of autophagy may be contributing to polyplex sequestration and subsequent lysosomal entrapment inside ARPE-19 cells. In future research it will be interesting to investigate if these LC3 positive compartments have sequestered previously released polyplexes in the cytosol or whether these compartments engulf whole endolysosomes, containing polyplexes. In any case, our results clearly indicate that xenophagy could be an important lead for further investigation.

Live-cell fluorescence colocalization microscopy holds great promise to elucidate the intracellular trafficking of nanomedicines. This method would further

profit from improved image quality and higher signal-to-noise ratios. The steady progress in developing fast and sensitive confocal imaging systems will certainly be helpful in that respect. Moreover, increased confocality would provide more power to selectively study colocalization events, close to the plasma membrane, for example, with clathrin-coated pits. Second, a transition to high-throughput/high content microscopy is desired for a more systematic screening of different types of particles and target cells, as well as to improve the statistical relevance of the data. In addition, simultaneous imaging of different endosomal markers and nanomedicines would allow visualization of overlap between different endosomal markers and define links between the different endosomal compartments used by endocytosed nanomedicines.

CONCLUSION

Nanomedicines with intracellular targets like nucleic acid delivery vehicles which are entering the target cell *via* endocytosis need efficient intracellular targeting to mediate their therapeutic effect. The mechanisms that direct endocytosis and further intracellular trafficking are generally dictated by the nature of the gene carrier and the target cell, and strongly determine final transfection efficiency. The complexity and dynamics of these mechanisms all contribute to the difficulty to predict intracellular processing of nanomedicines and the efficacy of their payload delivery. Therefore, robust and reliable tools are required to characterize and evaluate the intracellular processing of administered nanomedicines. In this work, we introduced a quantitative approach to study live-cell endosomal colocalization dynamics of nanomedicines for gene delivery, based on SPT and trajectory-correlation. In accordance with previous reports on nonviral gene complexes, our findings support the hypothesis that only a small fraction of polyplexes is able to escape the aggressive environment of the lysosomal organelles, indicating that endosomal release remains an important bottleneck for intracellular nucleic acid delivery. Moreover, we found direct evidence that xenophagy is involved in the persisting endosomal sequestration of the exogenous polyplexes. We conclude that dynamic colocalization is a promising tool to map and understand intracellular endosomal trafficking of nanomedicines. In future research it will allow the comparison of intracellular trafficking of different carriers or evaluate carrier modifications in different cell types, which should all aid the further development and design of effective nanomedicines.

METHODS

Materials. Dulbecco's modified Eagle's medium (DMEM), OptiMEM, L-glutamine, fetal bovine serum (FBS), penicillin-streptomycin solution (5000 IU/mL penicillin and 5000 μg/mL streptomycin) (P/S), and phosphate-buffered saline (PBS) were supplied by GibcoBRL (Merelbeke, Belgium). CellLight labeling kits (Endosomes, Lysosomes and Golgi), Tetraspeck microspheres of 200 nm, AlexaFluor647 (AF647)-labeled 10 kDa dextran and Lipofectamine2000 for gene transfection were purchased from Invitrogen (Merelbeke, Belgium). All other reagents were purchased from Sigma–Aldrich (Bornem, Belgium) unless otherwise stated.

Cell Culture. ARPE-19 cells (retinal pigment epithelial cell line; ATCC number CRL-2302) were cultured in DMEM:F12 supplemented with 10% FBS, 2 mm L-glutamine, and 2% P/S. All cells were grown at 37 °C in a humidified atmosphere containing 5% CO_2.

Plasmids. The plasmid constructs pGFP-Rab11 (p12674, Addgene) and pClathrin-light-chain-EYFP (p21741, Addgene) were a kind gift of P. Van Oostveldt (Ghent university, Belgium), pGFP-LC3 was a kind gift from P. Vandenabeele (VIB, Ghent, Belgium), pEGFP-Flot2 was a kind gift from B. Nichols (Cambridge University, UK) and pEGFP-Cav1 was a kind gift from M. Gumbleton (Cardiff University, UK). The plasmid constructs were all transformed in single step (KRX) competent cells (Promega, Leiden, The Netherlands) according to the manufacturer's instructions. The transformed bacteria were then selected for kanamycin resistance and grown to an OD of 1.5. The plasmids were isolated with a QIAfilter Plasmid Giga Kit (Qiagen, Venlo, The Netherlands) and concentrations were determined by UV absorption at 260 nm. Finally, the plasmids were suspended and stored in 25 mM HEPES, pH 7.2.

For fluorescent labeling of plasmid in the far red spectral range, pGL4.13 plasmid was labeled with Cy5 (Label IT Nucleic Acid Labeling Kit, Mirus Bio Corporation, WI, USA), according to the manufacturer's instructions at a 1:2 (v:w) ratio of Label IT Tracker Reagent and plasmid. To remove free label and salts, the plasmid was precipitated *via* addition of 2.5 volumes of ice-cold ethanol and 0.1 volume of 5 M NaCl. After incubation for 30 min at 4 °C, centrifugation at 17000*g* for 10 min and washing with ice-cold 70% ethanol, fluorescently labeled plasmid was finally resuspended in 25 mM HEPES, pH 7.2. The concentration of the plasmid was again determined by UV absorption at 260 nm.

Polyplexes. p(CBA-ABOL)/DNA complexes were obtained by adding a polymer solution of 0.6 mg/mL to a plasmid solution of 0.05 mg/mL in a final mass ratio of 48/1 in 25 mm HEPES buffer pH 7.2 and vortexing the mixture for 10 s. These gene complexes have in HEPES buffer an average hydrodynamic diameter of 120 nm and an average zeta potential of +40 mV. This was measured in undiluted samples of the polyplexes on a NanoZS zetasizer (Malvern Instruments, Hoeilaart, Belgium).

p(CBA-ABOL)/mRNA complexes were obtained using the same protocol as for p(CBA-ABOL)/DNA complexes. mRNA was produced with the help of the T7 mMessage kit for *in vitro* transcription of capped mRNA (Applied Biosystems/Ambion, Austin, USA). The used template was derived from the plasmid pGEM4Z-GFP-A64 after purification with the QIAquick PCR purification kit (Qiagen, Venlo, The Netherlands), linearization with the restriction enzyme SpeI, and a second purification with the QIAquick kit. The T7 mMessage kit was used according to the manufacturer's instructions. Briefly, linearized template DNA was mixed with buffer, nucleotide mix, and the T7 RNA polymerase, followed by an incubation period of 3 h at 37 °C. Next, the template DNA was enzymatically degraded and the mRNA was precipitated with LiCl. Purified mRNA was finally resuspended in nuclease-free 25 mM HEPES buffer, pH 7.2. The concentration of mRNA was determined by UV absorption at 260 nm.

Analysis of Transfection Efficiency of p(CBA-ABOL)/mRNA.GFP Polyplexes. Cells were seeded into 6-well plates (2×10^5 cells per

well) and allowed to attach overnight. Subsequently, the culture medium was removed and polyplexes, composed of pGEM4Z-GFP-A64-derived mRNA and p(CBA-ABOL), were added to the well (4 μg of mRNA per well). After every indicated time point, cells were washed with PBS and trypsinized. For all time points later than 2 h, the cells were washed at t = 2 h and further incubated in full cell culture medium. The average GFP expression of the total gated population of cells and the amount of GFP-positive cells in the same gate were subsequently measured by flow cytometry. As a negative control, cells were transfected with pGL4.13 plasmid since luciferase expression does not produce a detectable signal in the FL1 channel of the flow cytometer. A cell was considered GFP-positive and therefore successfully transfected if the individual fluorescence of the cell exceeded the threshold T, defined as the 99.5 percentile of the negative control sample.

Expression of Fluorescent Protein Constructs. ARPE-19 cells were seeded at a concentration of 220.000 cells per well on sterile MatTek coverslips (1.5)-bottom dishes (MatTek Corporation, MA, USA). The next day, cells were transfected with plasmids coding for the EGFP constructs GFP-Rab11, Clathrin-EYFP, EGFP-Flot2, EGFP-Cav1, EGFP-Rab7, and GFP-LC3 using Lipofectamine or with the CellLight staining kits, transducing GFP-Rab5, emGFP-LAMP1, or emGFP-*N*-acetyl-galactosaminyltransferase 2, according to the manufacturer's description. Briefly, for every Petri dish, 7 μL of Lipofectamine was mixed with 4 μg of plasmid in 500 μL of OptiMEM. After 30 min, this mixture was added to 1500 μL of OptiMEM on top of the cells. After 4 h, the cells were carefully washed and complete cell culture medium was applied. In the case of CellLight transduction, 50 μL of CellLight reagent was diluted 20x in full cell culture medium. The cells were then incubated overnight to allow expression of the fluorescent protein constructs.

Live-Cell Fluorescence Colocalization Microscopy. For dextran colocalization experiments, 0.5 mg/mL AF647-labeled dextran in OptiMEM was added for 15 min at 37 °C to the cells expressing fluorescent protein constructs. The cells were thoroughly washed with complete cell culture medium to reduce background fluorescence before live-cell imaging. For live-cell colocalization studies of p(CBA-ABOL) polyplexes, fresh polyplexes were diluted 5x in OptiMEM when added to the cells expressing fluorescent protein constructs, corresponding to 4 μg of Cy5-labeled plasmid. Intense contact with the cells was assured through repetitive pipetting at room temperature, allowing electrostatic adhesion of the polyplexes to the plasma membrane. Next, the cells were washed and imaged in fresh OptiMEM to chase the cell-associated fraction of polyplexes. For live-cell imaging, the cells were placed on the microscope in a stage top incubation chamber (Tokai Hit, Shizuoka, Japan), set at 37 °C, 5% CO_2, and 100% humidity. GFP transfected cells were chosen for imaging based on a relatively low expression level of GFP-constructs to minimize the possibility of a disturbed cell functioning. At every measured time point, a movie from a different cell was acquired to minimize photobleaching and phototoxicity, and to obtain information on a large population of cells.

All dual-color live-cell imaging for trajectory-based colocalization was performed on a custom-built laser widefield fluorescence microscope setup, here referred to as the single particle tracking or "SPT-microscope".[27] The SPT-microscope uses a TE2000-E inverted microscope equipped with a Plan Apo VC 100x 1.4 NA oil immersion objective lens (Nikon Belux, Brussels, Belgium). GFP was excited with a 491 nm laser line (Cobolt, Stockholm, Sweden), while Cy5 and AF647 were excited with a 636 nm diode laser (IQ1C, Power Technology, Little Rock, AR). The green emission channel is defined in a spectral range between 500 and 600 nm and the red channel between 655 and 745 nm. Green and red fluorescence images were registered simultaneously on separate halves of the chip of an electron-multiplying CCD (EMCCD) camera (Cascade II:512, Roper Scientific, Nieuwegein, The Netherlands). The videos were acquired in NIS Elements (Nikon Belux, Brussels, Belgium) at a frame speed of 2 frames per second and exposure times of 30−100 ms. The EMCCD camera was synchronized with an acousto-optical tunable filter (AOTF) to only illuminate the sample during the actual camera exposure time so as to minimize phototoxicity and photobleaching. The overlay of the green and the red channel was obtained with in-house developed software *via* acquisitions of stationary Tetraspeck microspheres, which were immobilized on a coverglass. These microspheres contain multiple fluorophores and can thus be detected in both the green and red channel, allowing calculation of the transformation parameters to overlay both channels.

To validate dynamic colocalization or correlated endosomal movement in living cells, 200 nm diameter polystyrene Tetraspeck microspheres were administered to ARPE-19 cells. Here, cells were seeded in MatTek coverslip dishes, 24 h before addition of the microspheres that were diluted 4000x in cell culture medium. These were then incubated for 3 h with the cells, after which the beads were washed away with cell culture medium and chased for another 2 h (to decrease the amount of cell-attached, noninternalized beads). Ten dual-color fluorescence movies were then recorded on the SPT-microscope. As a negative control experiment, ARPE-19 cells, expressing EGFP-LAMP1, were exposed shortly to Cy5-labeled p(CBA-ABOL) polyplexes and 10 dual-color movies were taken after 100 min of incubation. To obtain dual-color fluorescence movies without any correlated movement of fluorescent objects, the red channels (polyplexes) were randomly overlaid with the green channels (endosomes) from other cells.

Image Processing and Colocalization Analysis. Three methods were evaluated for quantitative colocalization analysis, respectively based on colocalization of pixels, objects and object trajectories. As earlier described by Braeckmans *et al*., first, a background removal was performed on all frames using an unsharp median filter with a kernel size of 15 pixels, followed by a median smoothing filter with a kernel size of 5 pixels for suppression of high-frequency noise.[41] These processed images were automatically thresholded and converted to binary images. These binary images were directly used for calculating pixel overlap. The pixel-based colocalization coefficient then represents the fraction of pixels from the red channel (polyplexes) that coincide with pixels from the green channel (endosomes).[42] The second method looks for the colocalization of identifiable objects. Here, the contours of individual fluorescent objects (endosomes and polyplexes) were first automatically identified in the binary image[41] and a red object (polyplex) was assigned as being colocalized with a green object (endosome) if the centroid of the red object was located within the contour of the green object.[42] The object-based colocalization coefficient was then determined as the fraction of red objects that is colocalized with green objects. The third, trajectory-based, method extends the principle of object-based colocalization, but also includes temporal information from the movie. As has been noted before, a convincing proof of object colocalization is their synchronized movement over several frames of a movie.[23] As explained in more detail in the Theory section of the Supporting Information, in this work we make use of this concept and propose a method for the quantitative analysis of correlated motion of objects. To this end, the motion trajectories of the identified green and red objects are first calculated as is typically done in SPT.[25,41,43] The dynamic, trajectory-based colocalization algorithm was implemented in custom-built software for detecting correlated movement between red and green objects (see also Supporting Information, Figure 1). The dynamic colocalization coefficient is then calculated as the fraction of red trajectories that show correlated movement with green trajectories. For the figures where the dynamic colocalization was plotted *versus* time, trend lines were calculated according to

$$\mu(t_n) = \frac{\sum_{i=n-4}^{n} N_{\mathrm{coloc}}(t_i)}{\sum_{i=n-4}^{n} N_{\mathrm{red}}(t_i)}$$

where $\mu(t_n)$ is the colocalization at time point t_n calculated as the average with the 4 preceding data points. $N_{\mathrm{coloc}}(t_i)$ is corresponding to the number of correlating red tracks in the movie, taken at time point t_i and $N_{\mathrm{red}}(t_i)$ to the total number of red

tracks in that same movie (after correction for stationary trajectories, see Supporting Information Results and supplemental Figure 3).

Acknowledgment. D. Vercauteren is a doctoral fellow of the Institute for the Promotion of Innovation through Science and Technology in Flanders (IWT), Belgium. We gratefully acknowledge the European Commission for funding through the Integrated 6th Framework Programme MediTrans. Financial support by the Ghent University Special Research Fund (Multidisciplinary Research Partnership NB-Photonics) and the Fund for Scientific Research Flanders are acknowledged with gratitude.

Supporting Information Available: Theory, supplementary results, supplementary figures, and supplementary movies. This material is available free of charge *via* the Internet at http://pubs.acs.org.

REFERENCES AND NOTES

1. Rajendran, L.; Knolker, H. J.; Simons, K. Subcellular Targeting Strategies for Drug Design and Delivery. *Nat. Rev. Drug Discovery* **2010**, *9*, 29–42.
2. Doherty, G. J.; McMahon, H. T. Mechanisms of Endocytosis. *Annu. Rev. Biochem.* **2009**, *78*, 31.1–31.46.
3. Stenmark, H. Rab GTPases as Coordinators of Vesicle Traffic. *Nat. Rev. Mol. Cell Biol.* **2009**, *10*, 513–525.
4. Luzio, J. P.; Pryor, P. R.; Bright, N. A. Lysosomes: Fusion and Function. *Nat. Rev. Mol. Cell Biol.* **2007**, *8*, 622–632.
5. Barua, S.; Rege, K. The Influence of Mediators of Intracellular Trafficking on Transgene Expression Efficacy of Polymer-Plasmid DNA Complexes. *Biomaterials* **2010**, *31*, 5894–5902.
6. Sahay, G.; Alakhova, D. Y.; Kabanov, A. V. Endocytosis of Nanomedicines. *J. Controlled Release* **2010**, *145*, 182–195.
7. Lechardeur, D.; Verkman, A. S.; Lukacs, G. L. Intracellular Routing of Plasmid DNA During Non-viral Gene Transfer. *Adv. Drug Delivery Rev.* **2005**, *57*, 755–767.
8. Suk, J. S.; Suh, J.; Lai, S. K.; Hanes, J. Quantifying the Intracellular Transport of Viral and Nonviral Gene Vectors in Primary Neurons. *Exp. Biol. Med.* **2007**, *232*, 461–469.
9. Comeau, J. W. D.; Costantino, S.; Wiseman, P. W. A Guide to Accurate Fluorescence Microscopy Colocalization Measurements. *Biophys. J.* **2006**, *91*, 4611–4622.
10. Bacallao, R.; Sohrab, S.; Phillips, C. Guiding Principles of Specimen Preservation for Confocal Microscopy. In *Handbook of Biological Confocal Microscopy*; Pawley, J. B., Ed.; Springer Science: New York, 2006; pp 368−380.
11. Richardson, S. C. W.; Wallom, K. L.; Ferguson, E. L.; Deacon, S. P. E.; Davies, M. W.; Powell, A. J.; Piper, R. C.; Duncan, R. The Use of Fluorescence Microscopy To Define Polymer Localisation to the Late Endocytic Compartments in Cells that Are Targets for Drug Delivery. *J. Controlled Release* **2008**, *127*, 1–11.
12. Shaner, N. C.; Steinbach, P. A.; Tsien, R. Y. A Guide to Choosing Fluorescent Proteins. *Nat. Methods* **2005**, *2*, 905–909.
13. Watson, P. Live Cell Imaging for Target and Drug Discovery. *Drug News Perspect.* **2009**, *22*, 69–79.
14. Naik, R.; Mukhopadhyay, A.; Ganguli, M. Gene Delivery to the Retina: Focus on Non-viral Approaches. *Drug Discovery Today* **2009**, *14*, 306–315.
15. Lin, C.; Zhong, Z. Y.; Lok, M. C.; Jiang, X. L.; Hennink, W. E.; Feijen, J.; Engbersen, J. F. J. Novel Bioreducible Poly(amido amine)s for Highly Efficient Gene Delivery. *Bioconjugate Chem.* **2007**, *18*, 138–145.
16. Lin, C.; Engbersen, J. F. J. The Role of the Disulfide Group in Disulfide-Based Polymeric Gene Carriers. *Expert Opin. Drug Delivery* **2009**, *6*, 421–439.
17. Christensen, L. V.; Chang, C. W.; Kim, W. J.; Kim, S. W.; Zhong, Z. Y.; Lin, C.; Engbersen, J. F. J.; Feijen, J. Reducible Poly(amido ethylenimine)s Designed for Triggered Intracellular Gene Delivery. *Bioconjugate Chem.* **2006**, *17*, 1233–1240.
18. Namgung, R.; Brumbach, J.; Jeong, J.; Yockman, J.; Kim, S.; Lin, C.; Zhong, Z.; Feijen, J.; Engbersen, J.; Kim, W. Dual Bio-Responsive Gene Delivery *via* Reducible Poly(amido amine) and Survivin-Inducible Plasmid DNA. *Biotechnol. Lett.* **2010**, *32*, 755–764.
19. Vader, P.; van der Aa, L.; Engbersen, J.; Storm, G.; Schiffelers, R. Disulfide-Based Poly(amido amine)s for siRNA Delivery: Effects of Structure on siRNA Complexation, Cellular Uptake, Gene Silencing and Toxicity. *Pharm. Res.* **2011**, *28*, 1013–1022.
20. Hoon Jeong, J.; Christensen, L. V.; Yockman, J. W.; Zhong, Z.; Engbersen, J. F. J.; Jong Kim, W.; Feijen, J.; Wan Kim, S. Reducible Poly(amido ethylenimine) Directed to Enhance RNA Interference. *Biomaterials* **2007**, *28*, 1912–1917.
21. Coué, G.; Engbersen, J. F. J. Functionalized Linear Poly(amidoamine)s Are Efficient Vectors for Intracellular Protein Delivery. *J. Controlled Release* **2011**, *152*, 90–98.
22. Vercauteren, D.; Piest, M.; van der Aa, L. J.; Al Soraj, M.; Jones, A. T.; Engbersen, J. F. J.; De Smedt, S. C.; Braeckmans, K. Flotillin-Dependent Endocytosis and a Phagocytosis-like Mechanism for Cellular Internalization of Disulfide-Based Poly(amido amine)/DNA Polyplexes. *Biomaterials* **2011**, *32*, 3072–3084.
23. Koyama-Honda, I.; Ritchie, K.; Fujiwara, T.; Iino, R.; Murakoshi, H.; Kasai, R. S.; Kusumi, A. Fluorescence Imaging for Monitoring the Colocalization of Two Single Molecules in Living Cells. *Biophys. J.* **2005**, *88*, 2126–2136.
24. Suh, J.; Dawson, M.; Hanes, J. Real-Time Multiple-Particle Tracking: Applications to Drug and Gene Delivery. *Adv. Drug Deliver Rev.* **2005**, *57*, 63–78.
25. Levi, V.; Gratton, E. Exploring Dynamics in Living Cells by Tracking Single Particles. *Cell Biochem. Biophys.* **2007**, *48*, 1–15.
26. Payne, C. K. Imaging Gene Delivery With Fluorescence Microscopy. *Nanomedicine (London)* **2007**, *2*, 847–860.
27. Braeckmans, K.; Buyens, K.; Bouquet, W.; Vervaet, C.; Joye, P.; De Vos, F.; Plawinski, L.; Doeuvre, L.; Angles-Cano, E.; Sanders, N. N.; *et al.* Sizing Nanomatter in Biological Fluids by Fluorescence Single Particle Tracking. *Nano Lett* **2010**, *10*, 4435–4442.
28. Baravalle, G.; Schober, D.; Huber, M.; Bayer, N.; Murphy, R. F.; Fuchs, R. Transferrin Recycling and Dextran Transport to Lysosomes is Differentially Affected by Bafilomycin, Nocodazole, and Low Temperature. *Cell Tissue Res.* **2005**, *320*, 99–113.
29. Szymanski, C. J.; Humphries, I. V.; Payne, C. K. Single Particle Tracking as a Method to Resolve Differences in Highly Colocalized Proteins. *Analyst* **2011**, *136*, 3527–3533.
30. Rejman, J.; Tavernier, G.; Bavarsad, N.; Demeester, J.; De Smedt, S. C. mRNA Transfection of Cervical Carcinoma and Mesenchymal Stem Cells Mediated by Cationic Carriers. *J. Controlled Release* **2010**, *147*, 385–391.
31. Deretic, V.; Levine, B. Autophagy, Immunity, and Microbial Adaptations. *Cell Host Microbe* **2009**, *5*, 527–549.
32. Levine, B. Eating Oneself and Uninvited Guests: Autophagy-Related Pathways in Cellular Defense. *Cell* **2005**, *120*, 159–162.
33. Yamaguchi, H.; Nakagawa, I.; Yamamoto, A.; Amano, A.; Noda, T.; Yoshimori, T. An Initial Step of GAS-Containing Autophagosome-like Vacuoles Formation Requires Rab7. *PLoS Pathog.* **2009**, *5*, 1–9.
34. Kirkegaard, K.; Taylor, M. P.; Jackson, W. T. Cellular Autophagy: Surrender, Avoidance and Subversion by Microorganisms. *Nat. Rev. Microbiol.* **2004**, *2*, 301–314.
35. Vieira, O. V.; Bucci, C.; Harrison, R. E.; Trimble, W. S.; Lanzetti, L.; Gruenberg, J.; Schreiber, A. D.; Stahl, P. D.; Grinstein, S. Modulation of Rab5 and Rab7 Recruitment to Phagosomes by Phosphatidylinositol 3-Kinase. *Mol. Cell. Biol.* **2003**, *23*, 2501–2514.
36. Strauss, O. The Retinal Pigment Epithelium in Visual Function. *Physiol Rev.* **2005**, *85*, 845–881.
37. Payne, C. K.; Jones, S. A.; Chen, C.; Zhuang, X. W. Internalization and Trafficking of Cell Surface Proteoglycans and Proteoglycan-Binding Ligands. *Traffic* **2007**, *8*, 389–401.
38. Langhorst, M. F.; Reuter, A.; Jaeger, F. A.; Wippich, F. M.; Luxenhofer, G.; Plattner, H.; Stuermer, C. A. O. Trafficking of

the Microdomain Scaffolding Protein Reggie-1/Flotillin-2. *Eur. J. Cell Biol.* **2008**, *87*, 211–226.
39. Iversen, T. G.; Skotland, T.; Sandvig, K. Endocytosis and Intracellular Transport of Nanoparticles: Present Knowledge and Need for Future Studies. *Nano Today* **2011**, *6*, 176–185.
40. Zhao, F.; Zhao, Y.; Liu, Y.; Chang, X.; Chen, C.; Zhao, Y. Cellular Uptake, Intracellular Trafficking, and Cytotoxicity of Nanomaterials. *Small* **2011**, *7*, 1322–1337.
41. Braeckmans, K.; Vercauteren, D.; Demeester, J.; De Smedt, S. C. Single Particle Tracking. In *Nanoscopy and Multidimensional Optical Fluorescence Microscopy*; Diaspro, A., Ed.; Taylor and Francis: New York, 2010; pp 5-1—5-17.
42. Bolte, S.; Cordelieres, F. P. A Guided Tour into Subcellular Colocalization Analysis in Light Microscopy. *J. Microsc.* **2006**, *224*, 213–232.
43. Wieser, S.; Schütz, G. J. Tracking Single Molecules in the Live Cell Plasma Membrane—Do's and Don't's. *Methods* **2008**, *46*, 131–140.